Current Research in Structural Biology 3 (2021) 206–215

Contents lists available at ScienceDirect

Current Research in Structural Biology

journal homepage: www.journals.elsevier.com/current-research-in-structural-biology

Room temperature crystallography of human acetylcholinesterase bound to a substrate analogue 4K-TMA: Towards a neutron structure

Oksana Gerlits [a], Matthew P. Blakeley [b], David A. Keen [c], Zoran Radić [d,**], Andrey Kovalevsky [e,*]

[a] Department of Natural Sciences, Tennessee Wesleyan University, Athens, TN, 37303, USA
[b] Large Scale Structures Group, Institut Laue–Langevin, 38000, Grenoble, France
[c] ISIS Facility, Rutherford Appleton Laboratory, Harwell Campus, Didcot, OX11 0QX, UK
[d] Skaggs School of Pharmacy and Pharmaceutical Sciences, University of California San Diego, La Jolla, CA, 92093-0751, USA
[e] Neutron Scattering Division, Oak Ridge National Laboratory, Oak Ridge, TN, 37831, USA

ARTICLE INFO

Handling Editor: Gabrielle Rudenko

Keywords:
X-ray diffraction
Neutron diffraction
hAChE
Room temperature
Reversible covalent inhibitor
4K-TMA

ABSTRACT

Acetylcholinesterase (AChE) catalyzes hydrolysis of acetylcholine thereby terminating cholinergic nerve impulses for efficient neurotransmission. Human AChE (hAChE) is a target of nerve agent and pesticide organophosphorus compounds that covalently attach to the catalytic Ser203 residue. Reactivation of inhibited hAChE can be achieved with nucleophilic antidotes, such as oximes. Understanding structural and electrostatic (i.e. protonation states) determinants of the catalytic and reactivation processes is crucial to improve design of oxime reactivators. Here we report X-ray structures of hAChE conjugated with a reversible covalent inhibitor 4K-TMA (4K-TMA:hAChE) at 2.8 Å resolution and of 4K-TMA:hAChE conjugate with oxime reactivator methoxime, MMB4 (4K-TMA:hAChE:MMB4) at 2.6 Å resolution, both at physiologically relevant room temperature, as well as cryo-crystallographic structure of 4K-TMA:hAChE at 2.4 Å resolution. 4K-TMA acts as a substrate analogue reacting with the hydroxyl of Ser203 and generating a reversible tetrahedral hemiketal intermediate that closely resembles the first tetrahedral intermediate state during hAChE-catalyzed acetylcholine hydrolysis. Structural comparisons of room temperature with cryo-crystallographic structures of 4K-TMA:hAChE and published mAChE complexes with 4K-TMA, as well as the effect of MMB4 binding to the peripheral anionic site (PAS) of the 4K-TMA:hAChE complex, revealed only discrete, minor differences. The active center geometry of AChE, already highly evolved for the efficient catalysis, was thus indicative of only minor conformational adjustments to accommodate the tetrahedral intermediate in the hydrolysis of the neurotransmitter acetylcholine (ACh). To map protonation states in the hAChE active site gorge we collected 3.5 Å neutron diffraction data paving the way for obtaining higher resolution datasets that will be needed to determine locations of individual hydrogen atoms.

1. Introduction

Acetylcholinesterase (AChE; EC 3.1.1.7), an α/β-hydrolase fold serine hydrolase, has evolved to catalyze termination of cholinergic nerve impulses at microsecond time-scale, allowing for efficient neurotransmission. As one of the premier biological catalysts it accelerates hydrolysis of neurotransmitter acetylcholine by an estimated 13 orders of magnitude (Quinn, 1987). This large scale enhancement is assumed to be enabled by specifics of the 3D structure of its ~ 65 kDa globular catalytic subunit where the tetrahedral intermediate in ACh hydrolysis finds near-perfect accommodation at the base of a narrow, 20 Å deep active center gorge lined with predominantly aromatic amino acid side chains. Notably, no structural evidence for any significant changes in conformations of the backbone or even side-chains have been found associated with its efficient catalytic cycle, as judged by modest diversity within more than 200 X-ray structures of AChEs obtained at cryo-temperatures (~100K) and available at the Protein Data Bank (PDB; wwPDB consortium, 2019). Crystallography at closer-to-physiological temperatures and solution-based techniques for determination of 3D structure still remain to be explored. AChE catalysis does not follow Michaelis-Menten kinetics what is particularly clear at millimolar concentrations of ACh. Although higher than needed for neurotransmission, millimolar concentrations appear physiologically feasible in its regulation. When crystallized at millimolar ACh, one ACh molecule is found bound in the opening of the

* Corresponding author.
** Corresponding author.
E-mail addresses: zradic@ucsd.edu (Z. Radić), kovalevskyay@ornl.gov (A. Kovalevsky).

https://doi.org/10.1016/j.crstbi.2021.08.003
Received 15 July 2021; Received in revised form 18 August 2021; Accepted 29 August 2021

AChE active center gorge at the peripheral anionic site (PAS) that presumably inhibits turnover of the other ACh in the active center resulting in „substrate inhibition“ (Bourne et al., 2006; Colletier et al., 2006). This hallmark of non-Michaelis-Menten kinetics of AChE is a likely consequence of its unique active center geometry and electronic configuration. To date, however, due to the absence of protonation details in X-ray diffraction-derived AChE structures, available 3D information has been restricted to the coordinates of heavy atoms obtained at cryo-temperatures.

X-ray crystallography has been routinely used in structural biology for structure-function studies and for structure-assisted drug design. Most of the biomacromolecular X-ray structures have been determined at cryo-temperatures using flash-frozen crystals. Cryo-crystallographic measurements are usually unavoidable, because significant radiation damage of small crystals (Garman, 2010) by the intense X-ray beams generated at synchrotron facilities may prevent diffraction data collection at the near-physiological (room) temperature, while large crystals can be difficult to grow. Cryo-temperature structures, however, may not provide representative conformational states of the protein or a ligand and may contain artifacts due to the required use of cryo-protectant chemicals and temperature effects (Fraser et al., 2011; Keedy et al., 2014; Kovalevsky et al., 2018; Otten et al., 2018; Gerlits et al., 2019a; Kneller et al., 2020). Therefore, room-temperature X-ray crystallography has gained appreciation in recent years. Recently, we demonstrated the value of room-temperature X-ray crystallography by showing productive reorientation of oxime reactivator RS-170B driven by the nerve agent VX conjugation of hAChE (Gerlits et al., 2019a). Nevertheless, positions of H atoms could not be resolved in any X-ray structures of AChE, leaving a significant gap in our understanding of the enzyme function, organophosphate inhibition and oxime reactivation. Neutron crystallography can fill this gap by accurately determining H atom positions and visualizing hydrogen bonding (Niimura and Podjarny, 2011; Niimura et al., 2016; O'Dell et al., 2016; Blakeley and Podjarny, 2018). Detection of H (and its heavier isotope deuterium, ^{2}H or D) atom locations hence permits direct determination of the protonation states. In addition, cold neutrons ($\lambda = \sim$2–5 Å) used in diffraction experiments cause no radiation damage to sensitive biological crystals so that neutron crystallographic data can be collected at room temperature. This is because electron clouds scatter X-rays, whereas atomic nuclei scatter neutrons; thus, unlike X-rays, neutrons do not ionize atoms. A drawback of neutron crystallography is the low neutron fluxes at neutron facilities compared to X-ray fluxes at synchrotrons requiring use of large crystals, normally 100-1000-fold larger than those typically used in X-ray diffraction. The crystal size can be reduced several-fold by protein (per)deuteration through expression in deuterated media, as the neutron scattering length of deuterium, D (^{2}H), is twice that of protium, ^{1}H (+6.671 fm *vs.* –3.739 fm, respectively). In addition, ^{1}H has a very large incoherent neutron scattering cross section that contributes only to background in neutron diffraction images, reducing the signal-to-noise ratio. Unfortunately, however, hAChE cannot be deuterated in its native, glycosylated form because mammalian cells used for the enzyme expression do not tolerate high levels of D_2O.

Catalytic hydrolysis of neurotransmitter acetylcholine (ACh) by AChE includes, minimally, initial formation of a reversible Michaelis-Menten complex, followed by short lived tetrahedral intermediate state where carbonyl carbon and Oγ of the catalytic triad Ser bind covalently, then by somewhat longer lived planar, acetylated AChE, followed by the second tetrahedral intermediate state that finally collapses into free, active AChE, available for the next round of catalytic hydrolysis. At high (millimolar) concentrations of ACh, catalytic hydrolysis is blocked by „substrate inhibition”. Several of the steps in the catalytic hydrolysis of ACh or its close thio-analogue acetylthiocholine (ATCh), have been already addressed by cryo-crystallographic X-ray analysis. Intact molecules of ACh and ATCh were found associated reversibly in the lower parts of both mouse AChE (mAChE) inactive S203A mutant (Bourne et al., 2006) and in native *Torpedo californica* AChE (TcAChE) inhibited by high substrate concentration (Colletier et al., 2006). In those complexes that could resemble geometry of Michaelis-Menten's complex, ACh/ATCh was stabilized in the choline binding site in an unusually curled conformation. It appears to be forced by an acetate molecule bound reversibly in the oxyanion hole, simultaneously with ACh/ATCh. The simultaneous presence of both acetate and ACh/ATCh is somewhat inconsistent/unexpected for the Michaelis-Menten catalytic step. Nevertheless, a covalent acetyl-AChE intermediate, was captured in TcAChE inhibited by both 20 mM and 500 mM ATCh (Colletier et al., 2006). Finally, a non-hydrolyzable ACh analogue 4K-TMA, was crystallized covalently linked to the active Ser in a tetrahedral configuration resembling the tetrahedral intermediate. An additional 4K-TMA molecule was modeled reversibly associated with PAS in a trigonal, planar configuration, both in mAChE and TcAChE (Bourne et al., 2006; Colletier et al., 2006), illustrating the association presumably responsible for inhibition by the substrate.

Here we report room-temperature X-ray structures of hAChE conjugated with a reversible covalent inhibitor 4K-TMA (4K-TMA:hAChE) at 2.8 Å resolution and of hAChE:4K-TMA conjugate with oxime reactivator methoxime, MMB4 (4K-TMA:hAChE:MMB4) at 2.6 Å resolution. A low-temperature structure of the 4K-TMA (4K-TMA:hAChE) complex at 2.4 Å resolution was also solved and included for comparison. 4K-TMA acts as a subtrate analogue whose ketone group reacts with the hydroxyl of the catalytic Ser203 to generate a metastable tetrahedral hemiketal intermediate (Fig. 1A). The hemiketal tetrahedral geometry closely resembles that of the first tetrahedral intermediate state during hAChE-catalyzed acetylcholine hydrolysis (Fig. 1B). Because the enzyme structure evolved around stabilizing the tetrahedral intermediate, detailed structural analysis of the 4K-TMA:hAChE complex obtained at close-to-physiological temperature is well justified. 4K-TMA:hAChE:MMB4 provides a mode of the oxime reactivator binding to the enzyme active site when the catalytic Ser203 residue is covalently inhibited. MMB4 binds at the peripheral anionic site (PAS) making π-π stacking interactions with Trp286 and does not protrude beyond Tyr124 choke point in the active site gorge. We compared 4K-TMA:hAChE complex with the cryo-temperature (100K) structures of apo-protomer in hAChE:LG703 complex (PDB ID 6U3P, Gorecki et al., 2020) and apo-hAChE (PDB ID 4EY4, Cheung et al., 2012), and also with mouse 4K-TMA:mAChE complex (Bourne et al., 2006) revealing structural differences in the active site cavities that can be explained by binding of the covalent reversible inhibitor or attributed to temperature effects. Conversely, binding of the MMB4 oxime to the 4K-TMA:hAChE complex does not perturb the conformation of the active site gorge. In addition, we were able to grow large 4K-TMA:hAChE crystals allowing a room-temperature neutron diffraction data collection to 3.5 Å resolution from an H/D-exchanged crystal in pursuit of a neutron structure of hAChE to visualize protonation states in the enzyme active site gorge.

2. Methods

2.1. Chemicals

4-ketoamyltrimethylammonium (4K-TMA) iodide was purchased from ICN and dissolved in water at 100 mM concentration. MMB4 was purchased from Millipore-Sigma (St. Louis, MO, USA) and dissolved in DMSO at 100 mM concentration. Protein purification supplies were purchased from GE Healthcare (Piscataway, New Jersey, USA). Crystallization reagents were purchased from Hampton Research (Aliso Viejo, California, USA). Crystallographic supplies were purchased from MiTeGen (Ithaca, New York, USA), Molecular Dimensions (Maumee, OH) and Vitrocom (Mountain Lakes, New Jersey, USA).

2.2. Expression and purification

The recombinant hAChE containing the N-terminal FLAG tag was expressed in the Gnt1- HEK293 mammalian cell culture deficient in

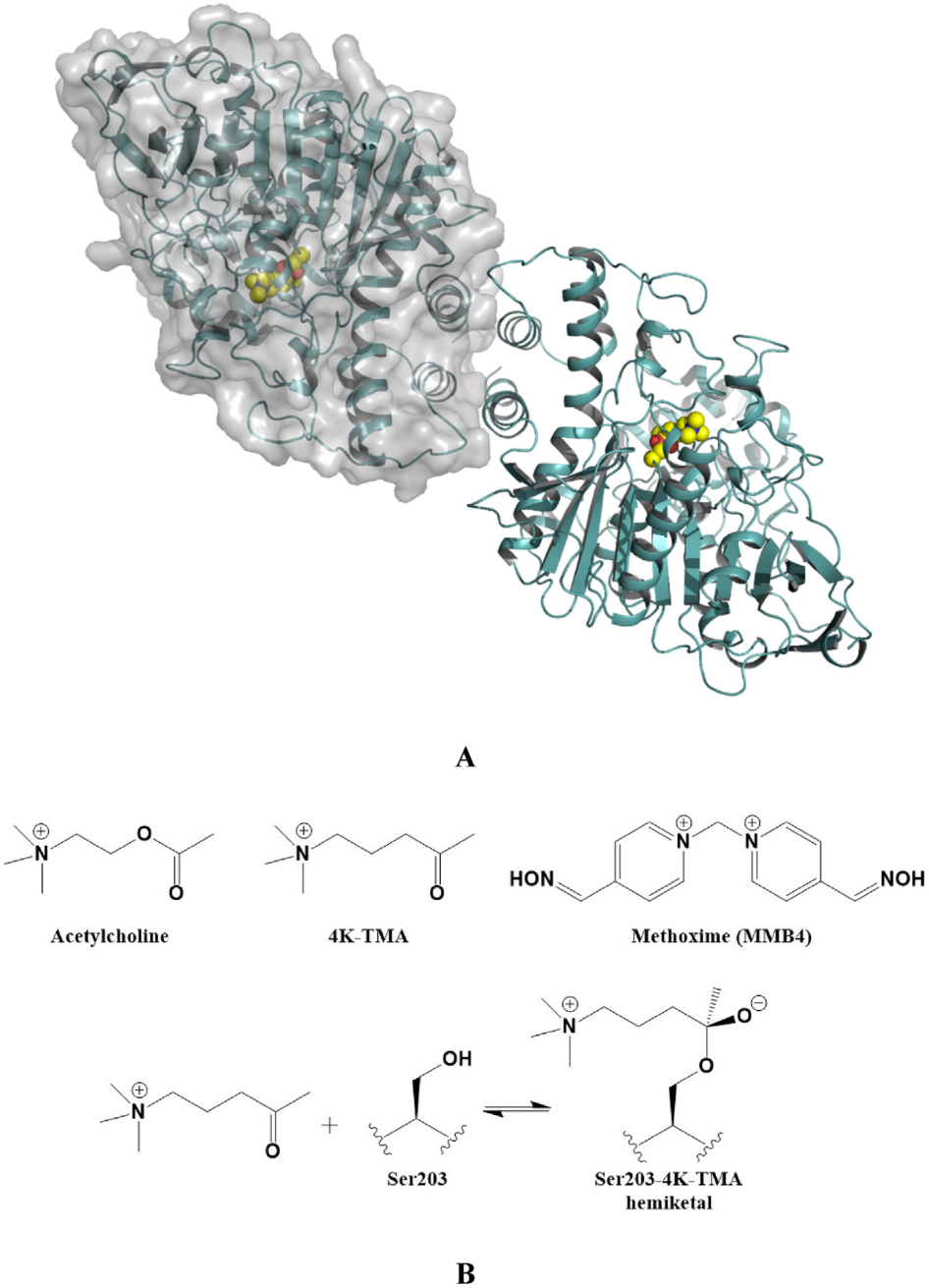

Fig. 1. (**A**) Human acetylcholinesterase (hAChE) four-helix bundle dimer in cartoon representation. Ser203-4K-TMA adduct bound in the active site is shown in ball-and-stick representation. (**B**) Chemical diagrams of substrate acetylcholine, its analogue 4K-TMA and the reaction of hAChE Ser203 residue with 4K-TMA to give the reversible hemiketal adduct.

complex N-glycans as previously described (Cochran et al., 2011). The enzyme was eluted from the anti-FLAG affinity column by specific human rhinovirus (HRV) 3C proteolysis (Sinobiological.com), cleaving the FLAG tag off at the engineered PreScission protease recognition site. Resulting N-terminal sequence of the pure eluted hAChE was G-P-L-**E-G-R-** … where amino acid sequence of the mature hAChE protein starts at **E-G-R-** … and ends at the truncated C-terminus with sequence … -S-A-T-D-T-L-D^{547}. Physiologically relevant hAChE dimers spontaneously and reversibly associate in solution from the expressed monomers.

2.3. Crystallization

For crystallization experiments a sample of hAChE was dialyzed in 10 mM HEPES, pH 7, 10 mM NaCl, and concentrated to 6–10 mg/mL. About 1 h prior to crystallization, the solution of hAChE was combined with a 100 mM stock solution of 4K-TMA in water at a molar ratio of 1:10 to obtain a binary reversible covalent complex of 4K-TMA:hAChE. The resultant sample was combined with the stock solution of MMB4 to generate a 10-fold molar excess of the oxime to hAChE producing the ternary 4K-TMA:hAChE:MMB4 complex. Crystals of both complexes were grown by vapor diffusion at 10 °C in sitting drops using Hampton Research 9-well glass plates and sandwich box setups for 4K-TMA:hAChE and Hampton Research microbridges for 4K-TMA:hAChE:MMB4. To grow neutron-quality crystals the crystallization drops were made by mixing 100 μL of 4K-TMA:hAChE solution with 100 μL of the well solution containing 100 mM HEPES, pH 7.5, 10 mM sodium citrate, and 6–8% PEG6000. The largest crystals grew to volumes of ~0.05–0.1 mm^3 in three months by slowly lowering the temperature from 10 °C to 6 °C

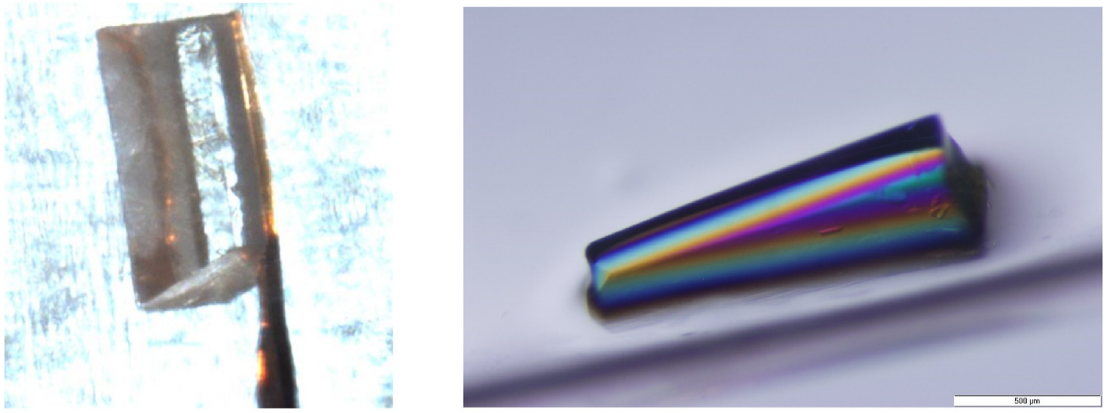

A

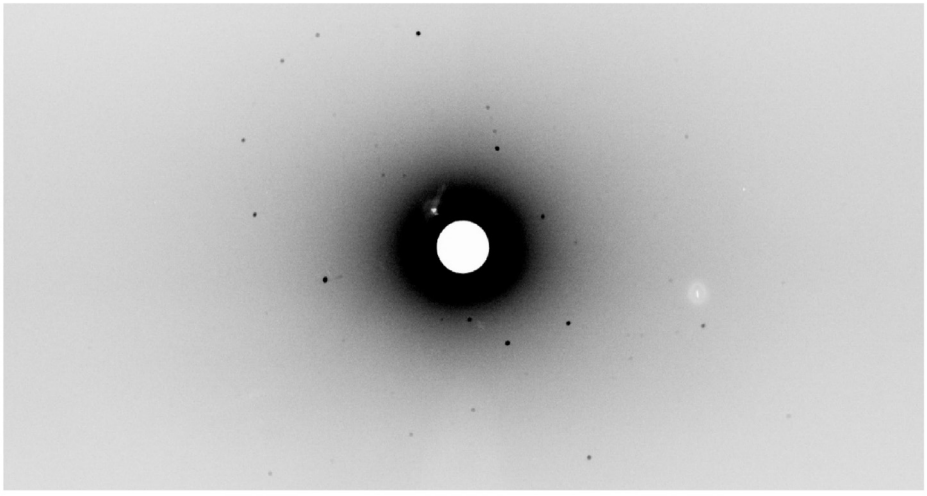

B

Fig. 2. (**A**) Photographs of the hAChE-4K-TMA crystals used to collect room-temperature X-ray (left, ~0.05 mm^3) and neutron (right, ~0.1 mm^3) diffraction datasets. (**B**) A representative neutron diffraction image from the H/D-exchanged crystal.

(Fig. 2A). The crystallization conditions were same for 4K-TMA:hAChE:MMB4 crystal growth, except for using 20 μL of the complex solution and 20 μL of the well solution to make the crystal drops.

2.4. X-ray diffraction data collection and structure refinement

Prior to the diffraction data collection crystals of 4K-TMA:hAChE or 4K-TMA:hAChE:MMB4 complexes were mounted on Molecular Dimensions elliptical Litholoops using the MiTeGen (Ithaca, NY) room-temperature capillary setups. Room temperature X-ray crystallographic data from 4K-TMA:hAChE were collected using a Rigaku HighFlux HomeLab instrument equipped with a MicroMax-007 HF X-ray generator and Osmic VariMax optics. The diffraction images were obtained using an Eiger R 4M hybrid photon counting detector. Diffraction data were integrated, reduced and scaled using the CrysAlis Pro software suite (Rigaku Inc., The Woodlands, TX). Room temperature diffraction data from 4K-TMA:hAChE:MMB4 were collected on the ID19 beamline at SBC-CAT using a Pilatus3 X 6M (ID19) detector at the Advanced Photon Source (APS). These data were integrated and scaled using the HKL3000 software suite (Minor et al., 2006). The structures were solved by molecular replacement using Phaser (McCoy et al., 2007) from the CCP4 program (Winn et al., 2011) and the starting model from PDB code 6O5R (Gerlits et al., 2017). The refinement of the protein structures was conducted using *Phenix.refine* (Afonine et al., 2012) from the Phenix (Adams et al., 2010; Liebschner et al., 2019) suite of programs and the COOT (Emsley et al., 2010) molecular graphics program. The geometry of each final structure was then carefully checked with Molprobity (Chen et al., 2010); the data collection and refinement statics are shown in Table 1.

2.5. Neutron diffraction data collection

The largest crystal of 4K-TMA:hAChE complex was mounted in a Vitrocom 2 mm-inner diameter quartz capillary containing a stabilizing solution made with 99.8% D_2O. H/D exchange was allowed to occur for 1 month before commencing neutron diffraction experiments. Neutron diffraction was tested at room temperature on the IMAGINE (Meilleur et al, 2013, 2018, 2020; Coates et al., 2018) instrument located at the High Flux Isotope Reactor (Oak Ridge National Laboratory) using the broad bandpass functionality with neutron wavelengths between 2.8 and 10 Å. The quasi-Laue neutron diffraction dataset to 3.5 Å resolution was then collected at room temperature on the LADI-III beamline at the Institut Laue-Langevin, Grenoble, France (Blakeley et al., 2010) using neutron wavelengths between 3.45 and 4.55 Å. A representative neutron diffraction image is shown in Fig. 2B. 22 images were collected from two different crystal orientations. At each orientation, the crystal was held

Table 1
Room temperature X-ray and neutron data collection statistics and X-ray structure refinement.

Data collection:	4K-TMA:hAChE Room temperature PDB ID 7RB5		4K-TMA:hAChE:MMB4 Room temperature PDB ID 7RB7	4K-TMA:hAChE 100K PDB ID 7RB6
	X-ray	**Neutron**	**X-ray**	**X-ray**
Beamline/Facility	Rigaku HighFlux HomeLab	LADI-III/ILL	ID19, Advanced Photon Source	ID19, Advanced Photon Source
Space group	$P3_112$		$P3_1$	$P3_1$
Cell dimensions:				
a, *b*, *c* (Å)	125.58, 125.58, 131.02		125.46, 125.46, 130.85	124.80, 124.80, 130.17
α, β, γ (°)	90, 90, 120		90, 90, 120	90, 90, 120
Resolution (Å)	40.00–2.80 (2.90–2.80)*	56.62–3.50 (3.69–3.50)*	40.00–2.60 (2.69–2.60)	40.00–2.40 (2.49–2.40)
No. reflections measured	99687	26732	185183	228390
No. reflections unique	28591 (2856)	8463 (977)	69461 (7031)	87262 (8730)
R_{merge}	0.100 (0.566)	0.285 (0.409)	0.050 (0.673)	0.065 (0.650)
$CC_{1/2}$	0.994 (0.551)		0.950 (0.404)	0.983 (0.543)
$I/\sigma I$	12.6 (1.7)	2.1 (1.1)	10.7 (1.4)	12.9 (1.7)
Completeness (%)	97.5 (97.2)	56.6 (45.4)	97.8 (98.4)	98.1 (98.5)
Redundancy	3.5 (3.6)	3.2 (2.2)	2.7 (2.7)	2.6 (2.6)
Refinement:				
Resolution	30 – 2.80		39.19 – 2.6	38.98 – 2.40
No. reflections	28581		63077	84333
R_{work}/R_{free}	0.195/0.233		0.190/0.214	0.182/0.215
No. atoms				
Protein	4188		8394	8396
Ligands	10		49	38
Water	56		1609	614
B-factors				
Protein	58.5		45.4	41.5
Ligand	41.5		54.7	45.7
Water	52.0		39.2	45.0
R.M.S. deviations				
Bond lengths (Å)	0.005		0.002	0.002
Bond angles (°)	0.685		0.469	0.560
Ramachandran statistics				
Favored	94.61		95.35	96.19
Allowed	5.20		4.55	3.81
Outliers	0.19		0.10	0
Clash score	3.62		2.53	2.58
Diffraction precision index	0.38		0.26	0.30

* - Values in parentheses are for highest resolution shell.

stationary at different ϕ settings for each 18-h exposure. The neutron data were processed using the Daresbury Laboratory LAUE suite program LAUEGEN modified to account for the cylindrical geometry of the detector (Campbell, 1995; Campbell et al., 1998). The program LSCALE (Arzt et al., 1999) was used to determine the wavelength-normalization curve using the intensities of symmetry-equivalent reflections measured at different wavelengths. No explicit absorption corrections were applied. These data were then merged in SCALA (Weiss, 2001). The summary of experimental data statistics is given in Table 1.

3. Results and discussion

3.1. Room temperature X-ray structure of hAChE:4K-TMA complex

hAChE devoid of the N-linked glycosylation at Asn350 and truncated at the amino acid residue 547 was expressed as a monomeric form in HEK293 cells (Cochran et al., 2011; Gerlits et al., 2017). The other two glycosylation sites Asn265 and Asn464 showed some electron density for the oligosaccharides, but could not be modeled in with confidence. Perhaps due to the lack of glycosylation at position 350 we are not able to grow diffraction-quality ligand-free (apo-) crystals of this recombinant hAChE. Therefore, to obtain crystals of hAChE:4K-TMA (4-ketoamyltrimethylammonium) complex, instead of soaking, we performed co-crystallization experiments by mixing the enzyme and the ligand solution prior to setting up crystallization drops. 4K-TMA is a non-hydrolyzable substrate analogue that produces a reversible hemiketal tetrahedral intermediate, when the carbonyl carbon reacts with the nucleophilic oxygen of the catalytic Ser203 side chain, in equilibrium with unreacted ketone (Fig. 1B).

Using a large crystal (~0.6 × 0.3 × 0.3 mm = 0.05 mm^3, Fig. 2) of hAChE:4K-TMA complex we collected a room-temperature X-ray diffraction dataset to 2.8 Å resolution on the in-house X-ray source (Table 1). There is clear electron density for the tetrahedral adduct covalently attached to the hydroxyl oxygen of Ser203 side chain, indicating that the hemiketal intermediate is trapped in the crystalline structure (Fig. 3A). We carefully examined the $2F_O$-F_C and difference F_O-F_C electron density maps and found no indication of radiation damage to the hemiketal of the covalently bound 4K-TMA adduct in our room-temperature structure. In contrast, the 4K-TMA adduct reportedly fell apart through radiolysis at 100K and 150K in the structures of *Torpedo californica* AChE:4K-TMA complex after irradiating the crystals with high doses of X-rays using a powerful synchrotron beam (Colletier et al., 2008). The quaternary ammonium group of 4K-TMA conjugate extends into the choline-binding site, adopting an almost perfect *trans, trans* conformation. The positively charged nitrogen makes classic cation-π interactions with the π-conjugated indole system of Trp86 with the shortest $N_{4K\text{-}TMA} \cdots C_\pi$ distance of 4.2 Å, whereas the methyl groups interact with Trp86 by means of C-H … π interactions as close as 3.5 Å (Dougherty, 2013; Plevin et al., 2010). The negative charge on the hemiketal oxygen is stabilized by three hydrogen bonds with the oxyanion hole formed by the main chain amide nitrogens of Gly121, Gly122, and Ala204, with distances of 2.6, 2.9 and 2.8 Å, respectively (Fig. 3A). The Ser203 side chain oxygen, now covalently bonded with 4K-TMA, makes a 2.7 Å hydrogen bond with imidazole of the catalytic His447. The methyl group of the hemiketal 4K-TMA faces the acyl pocket making hydrophobic contacts with the side chains of Phe295 and Phe297 similar to the interactions made by the corresponding methyl group in nerve agents VX and sarin (Allgardsson et al., 2016; Bester et al., 2018; Gerlits et al., 2019a).

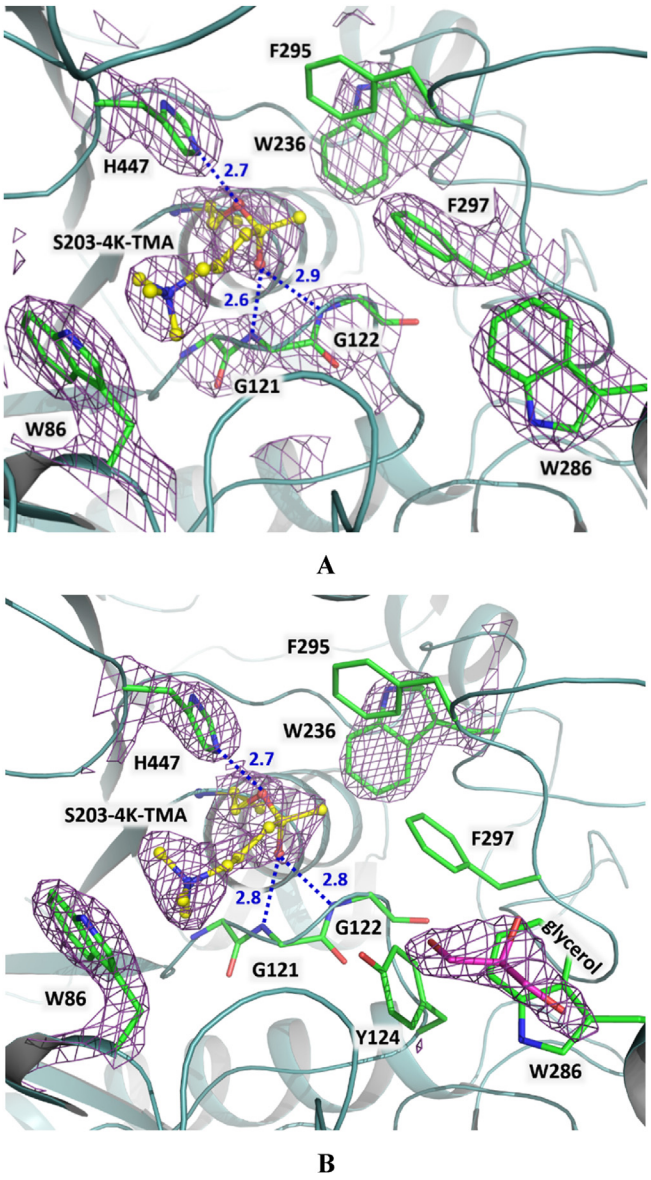

Fig. 3. hAChE active site in the covalent 4K-TMA:hAChE complex at room temperature (**A**, PDB ID 7RB5) and at 100K (**B**, PDB ID 7RB6). The substrate analogue ketone 4K-TMA reacts with the hydroxyl of Ser203 to generate a reversible tetrahedral hemiketal shown in ball-and-stick representation (yellow carbon atoms). The $2F_O$-F_C electron density is contoured at 2.0 σ level for hAChE residues, at 1.5 σ for 4K-TMA, and at 1.2 σ for glycerol. Hydrogen bonds are shown as blue dashed lines, with distances in Å. Hydrogen bond between the 4K-TMA oxyanion and the Ala204 main chain amide is omitted for clarity.

We did not observe a 4K-TMA molecule bound at the PAS in our room-temperature structure of hAChE:4K-TMA at 1.5 mM final 4K-TMA concentration consistent with its low binding affinity for this site ($K_d = 8.4$ mM; Bourne et al., 2006), although an intact 4K-TMA molecule was found at the PAS in *Tc*AChE:4K-TMA and mouse AChE:4K-TMA complexes using smaller ~0.5–1 mM 4K-TMA concentrations (Bourne et al., 2006; Colletier et al., 2006, 2008). We also obtained a 100K X-ray structure of hAChE:4K-TMA, in which we observed a glycerol molecule in the PAS centered above the Trp286 side chain imidazole (Fig. 3B). This observation is not surprising and it agrees with our previously determined structures of various hAChE complexes (Gerlits et al., 2019b; Gorecki et al., 2020), because the 4K-TMA:hAChE crystal was cryoprotected in a 2.7M glycerol, whereas for the cryoprotection of *Tc*AChE:4K-TMA and mAChE:4K-TMA crystals PEG200, which would not fit in the PAS, was used. Thus, glycerol likely outcompeted 4K-TMA from the PAS of hAChE attesting on low affinity of that interaction easily disturbed by the rise in temperature or by high concentration of a weak competitor.

3.2. Comparison of 4K-TMA: hAChE complex with the 100K apo-hAChE and mouse AChE:4K-TMA structures

The covalent binding of 4K-TMA ligand to the catalytic Ser203 does not dramatically alter the active site cavity of the enzyme, showing limited conformational changes (Fig. 4A). The room-temperature structure of the 4K-TMA:hAChE complex and the 100K structure of apo-hAChE (PDB ID 4EY4, Cheung et al., 2012) superimpose with a root mean square deviation (r.m.s.d.) of 0.7 Å for the main chain atoms. The position of the His447 side chain shifts slightly due to the presence of the covalent ligand, but imidazole maintains the hydrogen bond with Ser203. Trp86 and Trp236 that act as the walls of the choline binding site and the acyl pocket, respectively, move apart by ~0.6 Å to accommodate the hydrophobic groups of the 4K-TMA hemiketal. The most significant structural change in 4K-TMA:hAChE is the rotation of the Asp74 carboxylic group by ~29° moving one of its oxygens by 0.6 Å and a concurrent 0.9 Å shift of the Tyr341 phenolic group towards Asp74. Such conformational changes involving Asp74 and Tyr341 create a new 2.5 Å hydrogen bond between these two residues in the active site gorge of 4K-TMA:hAChE, which is absent in the apo-hAChE structure. Similar conformational changes are observed when 4K-TMA:hAChE is superimposed on the apo-protomer in hAChE:LG703 complex (Gorecki et al., 2020) (Fig. 4B). In the latter comparison, a small systematic (up to 0.5 Å) shift was also observed in Cα atoms of residues 75–79, in the Ω-loop capping the active center gorge, in both RT and LT structures of 4K-TMA:hAChE complex (Fig. 5A and B). The structures of the 4K-TMA:hAChE complex obtained at two different temperatures appear nearly identical, except for the minor surface loop difference (Fig. 5C).

It is also instructive to compare the room-temperature structure of hAChE:4K-TMA complex with the same complex of mouse AChE (mAChE) obtained at 100K (Fig. 4C). Similar to apo-hAChE structures, 4K-TMA complexes of mAChE and hAChE superimpose with an r.m.s.d. of 0.7 Å for the main chain atoms. Because 4K-TMA is already present in both structures, His447, Trp86 and Trp286 do not significantly change their positions. Interestingly, however, the hydrogen bond between Asp74 and Tyr341 is not formed in the mAChE:4K-TMA complex and the side chains of these two residues are >3.2 Å apart. Tyr337 shifts by 0.6 Å, whereas Trp286 in the peripheral anionic site moves only by 0.5 Å. Although it is unclear what causes the observed differences in the positions of Tyr337 in hAChE and mAChE complexes with 4K-TMA bound, the presence of the unreacted 4K-TMA in the peripheral anionic site in mAChE:4K-TMA complex can explain the shift of the Trp286 side chain. We suggest that the structural variations observed for Asp74, Tyr337 and Tyr341 side chains in the hAChE:4K-TMA and mAChE:4K-TMA structures may be attributed to temperature effects, as the structures were obtained at room temperature and 100K, respectively.

3.3. Room temperature X-ray structure of 4K-TMA:hAChE:MMB4 complex

The structure of 4K-TMA:hAChE:MMB4 complex was obtained using a synchrotron facility at 2.6 Å resolution, which is marginally better than the 2.8 Å resolution data collected for the 4K-TMA:hAChE complex using in-house instrumentation. In 4K-TMA:hAChE:MMB4, the observed electron density for the oxime reactivator allowed modeling of the whole molecule in protomer B of the enzyme, whereas only half of MMB4 could be modeled in protomer A. Therefore, the structure analysis is based on protomer B.

In 4K-TMA:hAChE:MMB4, 4K-TMA binds in exactly the same fashion as in 4K-TMA:hAChE, with the quaternary ammonium positioned in the choline-binding site, the methyl group in the acyl pocket and the

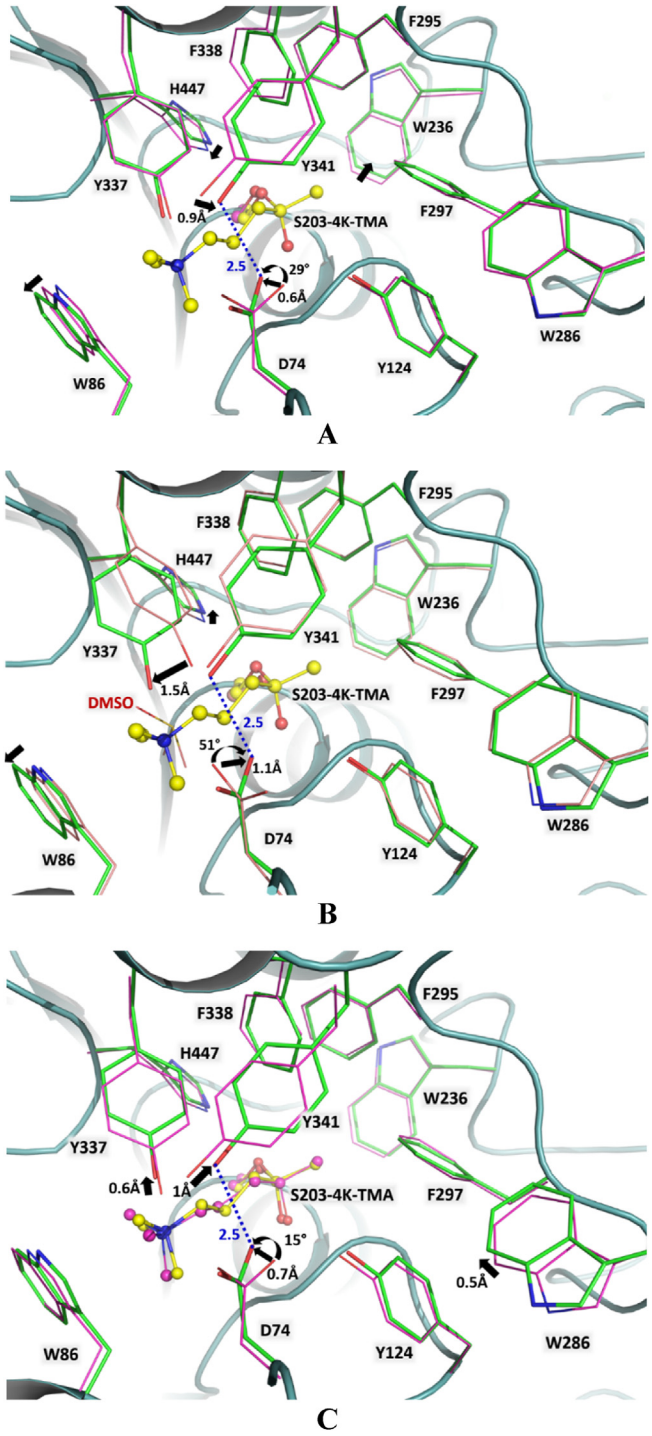

Fig. 4. Superposition of 4K-TMA:hAChE complex (PDB ID 7RB5, green and yellow carbon atoms) on apo-hAChE (PDB ID 4EY4, pink carbon atoms) (**A**), on the apo-protomer in hAChE:LG-703 complex (PDB ID 6U3P, salmon carbon atoms) (**B**) and on 4K-TMA:mAChE (PDB ID 2HA0, pink carbon atoms) (**C**). Hydrogen bonds are shown as blue dashed lines, with distances in Å. Shifts in the side chain positions are shown with black arrows.

hemiketal oxygen atoms forming hydrogen bonds with His447, Gly121 and Gly122 (Fig. 6). Half of the MMB4 reactivator binds at the PAS with one of its pyridinium rings making π-π stacking interactions of 3.4–3.7 Å with the Trp286 indole. The oxime group is directed towards the conjugated Ser203, but doesn't protrude beyond the 'choke point' formed largely by the Tyr124 side chain of the active site gorge. The oxime nitrogen and oxygen atoms are 3.5 and 3.7 Å away from the phenolic oxygen of Tyr124. The identical second half of the symmetric MMB4 molecule located outside of the active site gorge, is disordered and has little electron density. Binding of MMB4 causes virtually no effect on the hAChE structure, as 4K-TMA:hAChE and 4K-TMA:hAChE:MMB4 complexes superimpose with an r.m.s.d. of 0.17 Å on the main chain atoms. Some differences are seen in disordered/flexible surface loops (Fig. 5D). In addition, amino acid side chains in the active site gorge have no observable shifts upon the reactivator binding.

3.4. Room temperature neutron diffraction data

A neutron diffraction-quality crystal of 4K-TMA:hAChE complex was grown using a temperature-gradient methodology. Large crystallization drops of 200 μL in volume were initially set up at 10 °C. After the crystals were allowed to grow for one month, the crystallization temperature was gradually lowered to 6 °C over a period of another month. The crystallization trays were then kept at 6 °C for one more month. Crystal growth halted after about 3 months in total and the crystals did not become bigger when the temperature was reduced further to 4 °C. The largest crystal grew to a volume of ~0.1 mm^3; it was mounted in a quartz capillary using a stabilizing solution made with D_2O and allowed to exchange with deuterium for one month (Fig. 2A). Neutron diffraction data were collected using the quasi-Laue technique on the nuclear reactor-based LADI-III beamline at the Institut Laue-Langevin. The crystal diffracted to 3.5 Å resolution (Fig. 2B). The neutron data collection and processing statistics are given in Table 1.

This work marks the first room-temperature neutron crystallographic experiment on AChE enzyme from any species, although the experimental resolution does not permit us to locate individual hydrogen atoms in the enzyme structure. The neutron diffraction resolution (3.5 Å) is limited both by the size of the crystal we were able to grow, its diffraction quality as demonstrated by the resolution of the X-ray diffraction data set (2.8 Å), and the low neutron flux of current neutron diffraction beamlines. hAChE crystals are notoriously difficult to obtain and are known for their low-resolution diffraction, even in cryo-X-ray crystallographic experiments (Cheung et al., 2012; Franklin et al., 2016; Gerlits et al., 2019a, 2019b, 2019b; Gorecki et al., 2020). One reason for the poor diffraction quality of hAChE crystals is their high solvent content, which is often more than 70%. We envision that improvements in the crystal growth and in neutron diffraction instrumentation such as DALI at the Institut Laue Langevin, EWALD at the Second Target Station (ORNL) and NMX at the European Spallation Source will allow us to collect future neutron diffraction data sets from hAChE to higher resolution (Coates and Robertson, 2017; Marko et al., 2020).

4. Concluding remarks

The room-temperature structure of 4K-TMA conjugated hAChE mimicking the short-lived tetrahedral intermediate in the catalytic hydrolysis of ACh, resembles the cryo-temperature 4K-TMA:hAChE structure, as well as structures previously solved with mAChE and *Tc*AChE at cryo-temperatures. In spite of higher 4K-TMA concentration (~1.5 mM) used in our hAChE co-crystallization compared to mAChE co-crystals (~0.9 mM) or to *Tc*AChE (0.5 mM 4K-TMA in soaking), we have not observed any planar 4K-TMA or any other ligand at the PAS of hAChE. In our cryo-temperature 4K-TMA:hAChE structure glycerol was found bound at the PAS. That is consistent with high K_d of 4K-TMA determined for the PAS (Bourne et al., 2006). Binding of aldoxime MMB4 to the hAChE conjugate with 4K-TMA did not affect conformation of the conjugate at room temperature. The geometry and nature of interactions of the tetrahedral intermediate mimick thus remain undisturbed by either somewhat enhanced protein dynamics in crystals at the room temperature or by low affinity ligand binding at the PAS of hAChE. We thus conclude that the large magnitude of catalytic acceleration in ACh turnover by hAChE comes from its highly evolved active center geometry and electronics where the tetrahedral intermediate of ACh fits perfectly

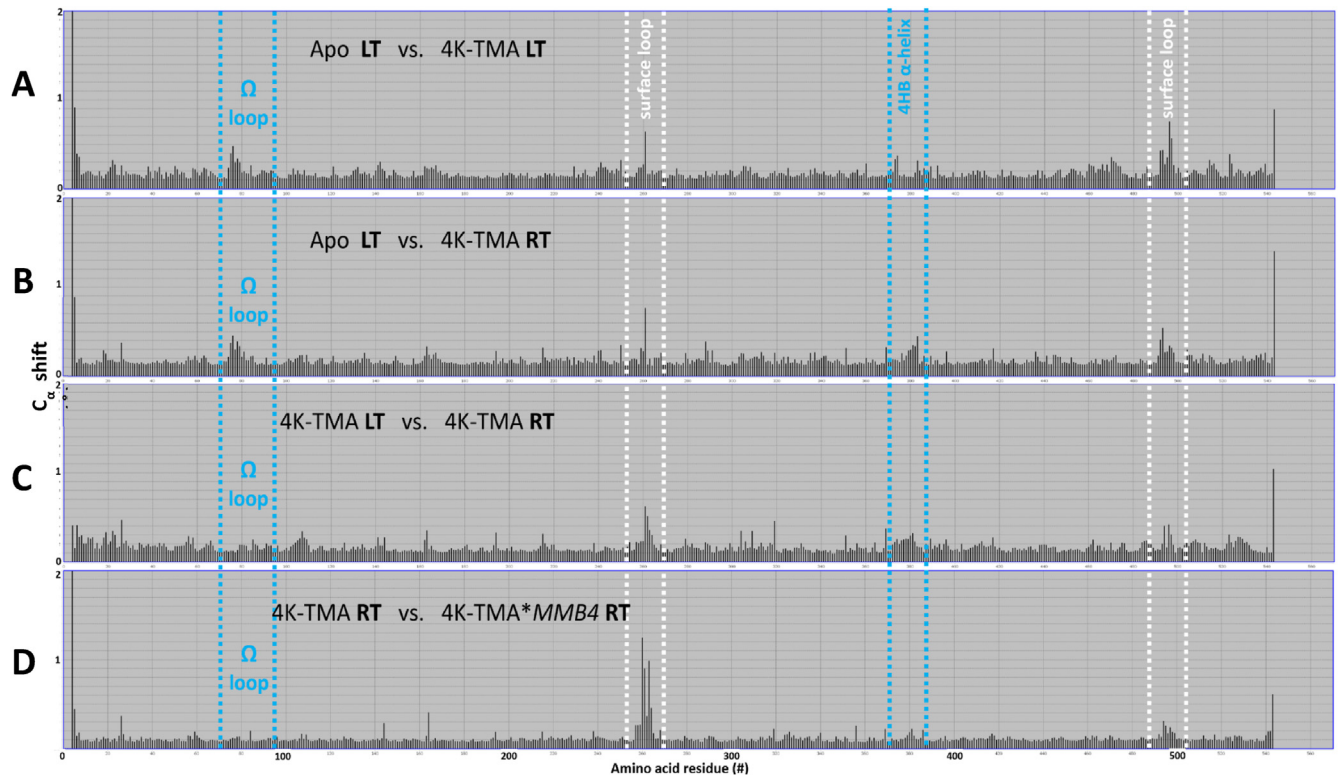

Fig. 5. Pairwise comparison of backbone C_α positions in 4K-TMA*hAChE complexes: **A**) comparison of **RT** 4K-TMA complex (PDB ID 7RB5) with unoccupied, apo hAChE structure *(PDB ID 6U3P:B)*; **B**) comparison of **LT** 4K-TMA complex (PDB ID 7RB6) with unoccupied, Apo hAChE structure *(PDB ID 6U3P:B)*; **C**) influence of data collection temperature LT (100 K) vs. RT (295 K); **D**) influence of occupation of PAS by MMB4, at RT. Position of relevant secondary structure elements, Ω loop covering active center gorge, C-terminally located 4HB α-helix and two surface loops with pronounced flexibility are indicated by vertical dashed lines. Comparison was done using PACCT (Pairwise Alpha Carbon Comparison Tool) available on www.ZENODO.org, DOI 10.5281/zenodo. 3992329.

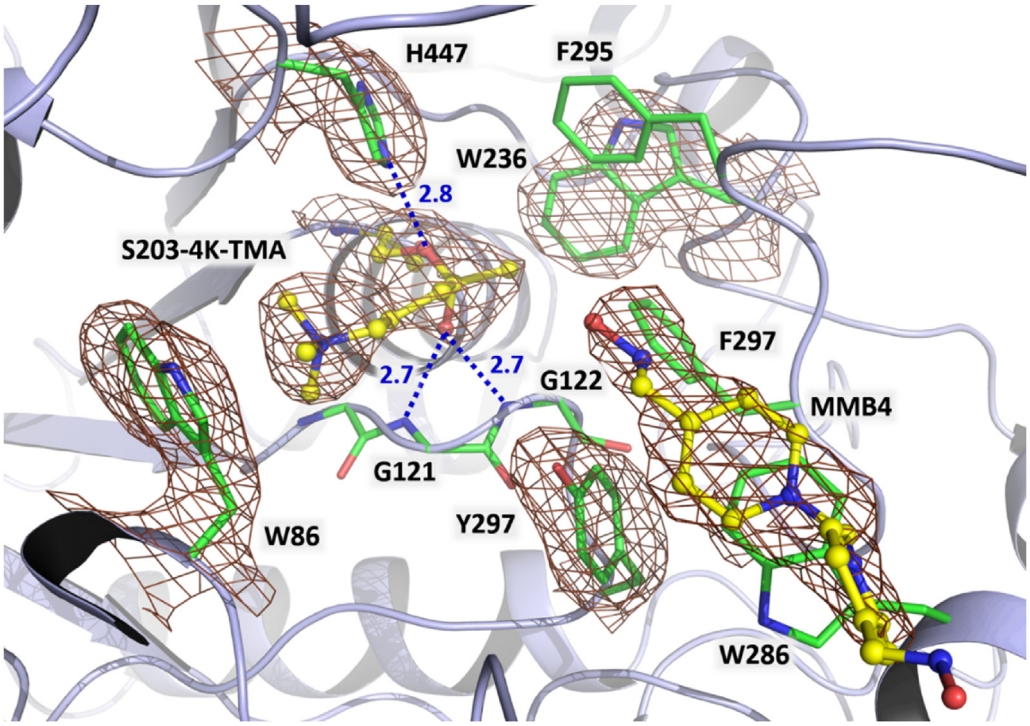

Fig. 6. Active site in the ternary 4K-TMA:hAChE:MMB4 complex at room temperature (PDB ID 7RB7). The substrate analogue hemiketal is shown in ball-and-stick representation (yellow carbon atoms). The $2F_O$-F_C electron density is contoured at 1.5 σ level (1.0 σ level for MMB4). Hydrogen bonds are shown as blue dashed lines, with distances in Å. Hydrogen bond between the 4K-TMA oxyanion and the Ala204 main chain amide is omitted for clarity.

well, without the need for any conformational adjustments that would require an input of energy. This is even consistent with observations in active centers of catalytically closely related yet structurally slightly more diverse cholinesterases: secondary isotope effect experiments in *Drosophila melanogaster* AChE (Tormos et al., 2010) and with X-ray structures of tetrahedrally distorted ligands stabilized by active serine in human butyrylcholinesterase (PDB IDs 1P0I and 6XYY, Nicolet et al., 2003). For hAChE, some conformational "breathing" of the narrowest upper part of the active center gorge may be necessary to facilitate diffusion of ACh towards the wider catalytic triad-containing base. These oscillations are likely to occur in a short (sub-μs) time-frame, are not limiting in the catalytic cycle and are insufficiently stable to be captured by X-ray crystallography, even at room temperature. Under our experimental conditions we have not detected radiation damage to the covalently bound 4K-TMA and, thus, did not observe any possible "back door" exit of hydrolysis products previously reported in a "shoot-and-trap" temperature-controlled cryo-crystallography X-ray analysis approach (Colletier et al., 2008). With the first collection of neutron diffraction data of any AChE at 3.5 Å resolution we are paving the way towards resolving positions of protons in the active center of hAChE captured in a tetrahedral intermediate step, critical for achieving exquisite catalytic power in the catalytic mechanism of this enzyme.

Funding information

This research was supported by the CounterACT Program, National Institutes of Health Office of the Director (NIH OD), and the National Institute of Neurological Disorders and Stroke (NINDS), [Grant Number U01 NS083451].

CRediT authorship contribution statement

Oksana Gerlits: Conceptualization, Methodology, Validation, Investigation, Writing – original draft. **Matthew P. Blakeley:** Formal analysis, Resources, Data curation. **David A. Keen:** Formal analysis, Resources, Data curation. **Zoran Radić:** Conceptualization, Validation, Writing – review & editing, Supervision, Project administration, Funding acquisition. **Andrey Kovalevsky:** Validation, Formal analysis, Resources, Data curation, Writing – original draft, Writing – review & editing, Visualization, Supervision.

Declaration of competing interest

The authors declare that they have no known competing financial interests or personal relationships that could have appeared to influence the work reported in this paper.

Acknowledgments

The Office of Biological and Environmental Research supported research at the Center for Structural Molecular Biology (CSMB) at ORNL using facilities supported by the Scientific User Facilities Division, Office of Basic Energy Sciences, U.S. Department of Energy. This research using IMAGINE beamline at the Oak Ridge National Laboratory's (ORNL) High Flux Isotope Reactor (HFIR) was sponsored by the Scientific User Facilities Division, Office of Basic Energy Sciences, U.S. Department of Energy. We thank the Institut Laue-Langevin (ILL, Grenoble, France) for awarding neutron beamtime on the neutron diffraction beamline LADI-III.

References

Adams, P.D., Afonine, P.V., Bunkoczi, G., Chen, V.B., Davis, I.W., Echols, N., Headd, J.J., Hung, L.W., Kapral, G.J., Grosse-Kunstleve, R.W., McCoy, A.J., Moriarty, N.W., Oeffner, R., Read, R.J., Richardson, D.C., Richardson, J.S., Terwilliger, T.C., Zwart, P.H., 2010. PHENIX: a comprehensive Python-based system for macromolecular structure solution. Acta Crystallogr. D Biol. Crystallogr. 66 (Pt 2), 213–221.

Afonine, P.V., Grosse-Kunstleve, R.W., Echols, N., Headd, J.J., Moriarty, N.W., Mustyakimov, M., Terwilliger, T.C., Urzhumtsev, A., Zwart, P.H., Adams, P.D., 2012. Towards automated crystallographic structure refinement with *phenix. refine*. Acta Cryst. D68, 352–367.

Allgardsson, A., Berg, L., Akfur, C., Hörnberg, A., Worek, F., Linusson, A., Ekström, F.J., 2016. Structure of a prereaction complex between the nerve agent sarin, its biological target acetylcholinesterase, and the antidote HI-6. Proc. Natl. Acad. Sci. Unit. States Am. 113, 5514–5519.

Arzt, S., Campbell, J.W., Harding, M.M., Hao, Q., Helliwell, J.R., 1999. LSCALE - the new normalization, scaling and absorption correction program in the Daresbury Laue software suite. J. Appl. Crystallogr. 32, 554–562.

Bester, S.M., Guelta, M.A., Cheung, J., Winemiller, M.D., Bae, S.Y., Myslinski, J., Pegan, S.D., Height, J.J., 2018. Structural insights of stereospecific inhibition of human acetylcholinesterase by VX and subsequent reactivation by HI-6. Chem. Res. Toxicol. 31, 1405–1417.

Blakeley, M.P., Podjarny, A.D., 2018. Neutron macromolecular crystallography. Emerg. Topics Life Sci. 2, 39–55.

Blakeley, M.P., Teixeira, S.C.M., Petit-Haertlein, I., Hazemann, I., Mitschler, A., Haertlein, M., Howard, E., Podjarny, A.D., 2010. Neutron macromolecular crystallography with LADI-III. Acta Crystallogr. D 66, 1198–1205.

Bourne, Y., Radic, Z., Sulzenbacher, G., Kim, E., Taylor, P., Marchot, P., 2006. Substrate and product trafficking through the active site center gorge of acetylcholinesterase analyzed by crystallography and equilibrium binding. J. Biol. Chem. 281, 29256–29267.

Campbell, J.W., 1995. LAUEGEN, an X-Windows-based program for the processing of Laue diffraction data. J. Appl. Crystallogr. 28, 228–236.

Campbell, J.W., Hao, Q., Harding, M.M., Nguti, N.D., Wilkinson, C., 1998. LAUEGEN version 6.0 and INTLDM. J. Appl. Crystallogr. 31, 496–502.

Chen, V.B., Arendall, W.B., Headd, J.J., Keedy, D.A., Immormino, R.M., Kapral, G.J., Murray, L.W., Richardson, J.S., Richardson, D.C., 2010. MolProbity: all-atom structure validation for macromolecular crystallography. Acta Crystallogr. D 66, 12–21.

Cheung, J., Rudolph, M.J., Burshteyn, F., Cassidy, M.S., Gary, E.N., Love, J., Franklin, M.C., 2012. Height, J. J. Structures of human acetylcholinesterase in complex with pharmacologically important ligands. J. Med. Chem. 55, 10282–10286.

Coates, L., Cao, H.B., Chakoumakos, B.C., Frontzek, M.D., Hoffmann, C., Kovalevsky, A.Y., Liu, Y., Meilleur, F., dos Santos, A.M., Myles, D.A.A., Wang, X.P., Ye, F., 2018. A suite-level review of the neutron single-crystal diffraction instruments at Oak Ridge National Laboratory. Rev. Sci. Instrum. 89, 092802.

Coates, L., Robertson, L., 2017. Ewald: an extended wide-angle Laue diffractometer for the second target station of the Spallation Neutron Source. J. Appl. Crystallogr. 50, 1174–1178.

Cochran, R., Kalisiak, J., Küçükkilinç, T., Radic, Z., Garcia, E., Zhang, L., Ho, K.Y., Amitai, G., Kovarik, Z., Fokin, V.V., Sharpless, K.B., Taylor, P., 2011. Oxime-assisted acetylcholinesterase catalytic scavengers of organophosphates that resist aging. J. Biol. Chem. 286, 29718–29724.

Colletier, J.-P., Fournier, D., Greenblatt, H.M., Stojan, J., Sussman, J.L., Zaccai, G., Silman, I., Weik, M., 2006. Structural insights into substrate traffic and inhibition in acetylcholinesterase. EMBO J. 25, 2746–2756.

Colletier, J.-P., Bourgeois, D., Sanson, B., Fournier, D., Sussman, J.L., Silman, I., Weik, M., 2008. Shoot-and-trap: use of specific X-ray damage to study structural protein dynamics by temperature-controlled cryo-crystallography. Proc. Natl. Acad. Sci. U.S.A. 105, 11742–11747.

Dougherty, D.A., 2013. The cation-π interaction. Acc. Chem. Res. 46, 885–893.

Emsley, P., Lohkamp, B., Scott, W.G., Cowtan, K., 2010. Features and development of coot. Acta Crystallogr. D Biol. Crystallogr. 66 (Pt 4), 486–501.

Franklin, M.C., Rudolph, M.J., Ginter, C., Cassidy, M.S., Cheung, J., 2016. Structures of paraoxon-inhibited human acetylcholinesterase reveal perturbations of the acyl loop and the dimer interface. Prot. Struct. Funct. Bioinform. 84, 1246–1256.

Fraser, J.S., van den Bedem, H., Samelson, A.J., Lang, P.T., Holton, J.M., Echols, N., Alber, T., 2011. Accessing protein conformational ensembles using room-temperature X-ray crystallography. Proc. Natl. Acad. Sci. U.S.A. 108, 16247–16252.

Garman, E.F., 2010. Radiation damage in macromolecular crystallography: what is it and why should we care? Acta Crystallogr. D 66, 339–351.

Gerlits, O., Keen, D.A., Blakeley, M.P., Louis, J.M., Weber, I.T., Kovalevsky, A., 2017. Room temperature neutron crystallography of drug resistant HIV-1 protease uncovers limitations of X-ray structural analysis at 100K. J. Med. Chem. 60, 2018–2025.

Gerlits, O., Kong, X., Cheng, X., Wymore, T., Blumenthal, D.K., Taylor, P., Radic, Z., Kovalevsky, A., 2019a. Productive reorientation of a bound oxime reactivator revealed in room temperature X-ray structures of native and VX-inhibited human acetylcholinesterase. J. Biol. Chem. 294, 10607–10618.

Gerlits, O., Ho, K.-Y., Cheng, X., Blumenthal, D., Taylor, P., Kovalevsky, A., Radic, Z., 2019b. A new crystal form of human acetylcholinesterase for exploratory room-temperature crystallography studies. Chem. Biol. Interact. 309, 108698.

Gorecki, L., Gerlits, O., Kong, X., Cheng, X., Blumenthal, D.K., Taylor, P., Ballatore, C., Kovalevsky, A., Radic, Z., 2020. Rational design, synthesis, and evaluation of uncharged, "smart" bis-oxime antidotes of organophosphate-inhibited human acetylcholinesterase. J. Biol. Chem. 295, 4079–4092.

Keedy, D.A., van den Bedem, H., Sivak, D.A., Petsko, G.A., Ringe, D., Wilson, M.A., Fraser, J.S., 2014. Crystal cryocooling distorts conformational heterogeneity in a model Michaelis complex of DHFR. Structure 22, 899–910.

Kneller, D.W., Phillips, G., O'Neill, H.M., Jedrzejczak, R., Stols, L., Langan, P., Joachimiak, A., Coates, L., Kovalevsky, A., 2020. Structural plasticity of SARS-CoV-2

3CL Mpro active site cavity revealed by room temperature X-ray crystallography. Nat. Commun. 11, 3202.
Kovalevsky, A., Aggarwal, M., Velazquez, H., Cuneo, M.J., Blakeley, M.P., Weiss, K.L., Smith, J.C., Fisher, S.Z., McKenna, R., 2018. 'To be or not to be' protonated: atomic details of human carbonic anhydrase-clinical drug complexes by neutron crystallography and simulation. Structure 26, 383–390 e3.
Liebschner, D., Afonine, P.V., Baker, M.L., Bunkoczi, G., Chen, V.B., Croll, T.I., Hintze, B., Hung, L.-W., Jain, S., McCoy, A.J., Moriarty, N.W., Oeffner, R.D., Poon, B.K., Prisant, M.G., Read, R.J., Richardson, J.S., Richardson, D.C., Sammito, M.D., Sobolev, O.V., Stockwell, D.H., Terwilliger, T.C., Urzhumtsev, A.G., Videau, L.L., Williams, C.J., Adams, P.D., 2019. Macromolecular structure determination using X-rays, neutrons and electrons: recent developments in *Phenix*. Acta Crystallogr. D75, 861–877.
Marko, M., Nagy, G., Aprigliano, G., Oksanen, E., 2020. Neutron macromolecular crystallography at the European spallation source. Methods Enzymol. 634, 125–151.
McCoy, A.J., Grosse-Kunstleve, R.W., Adams, P.D., Winn, M.D., Storoni, L.C., Read, R.J., 2007. *Phaser* crystallographic software. J. Appl. Crystallogr. 40, 658–674.
Meilleur, F., Kovalevsky, A., Myles, D.A.A., 2020. IMAGINE: the neutron protein crystallography beamline at the high flux isotope reactor. Methods Enzymol. 634, 69–85.
Meilleur, F., Coates, L., Cuneo, M.J., Kovalevsky, A., Myles, D.A.A., 2018. The neutron macromolecular crystallography instruments at Oak Ridge National Laboratory: advances, challenges, and opportunities. Crystals 8, 388.
Meilleur, F., Munshi, P., Robertson, L., Stoica, A.D., Crow, L., Kovalevsky, A., Koritsanszky, T., Chakoumakos, B.C., Blessing, R., Myles, D.A.A., 2013. The IMAGINE instrument: first neutron protein structure and new capabilities for neutron macromolecular crystallography. Acta Crystallogr. D69, 2157–2160.
Minor, W., Cymborowski, M., Otwinowski, Z., Chruszcz, M., 2006. HKL-3000: the integration of data reduction and structure solution–from diffraction images to an initial model in minutes. Acta Crystallogr. D 62, 859–866.
Nicolet, Y., Lockridge, O., Masson, P., Fontecilla-Camps, J.C., Nachon, F., 2003. Crystal structure of human butyrylcholinesterase and of its complexes with substrate and products. J. Biol. Chem. 278, 41141–41147.
Niimura, N., Podjarny, A., 2011. Neutron Protein Crystallography. Oxford University Press, p. 250.
Niimura, N., Takimoto-Kamimura, M., Tanaka, I., 2016. Neutron diffraction in studies of protein dynamics and functions, Application of. Encycl. Analyt. Chem. 1–30.
O'Dell, W.B., Bodenheimer, A.M., Meilleur, F., 2016. Neutron protein crystallography: a complementary tool for locating hydrogens in proteins. Arch. Biochem. Biophys. 602, 48–60.
Otten, R., Liu, L., Kenner, L.R., Clarkson, M.W., Mavor, D., Tawfik, D.S., Kern, D., Fraser, J.S., 2018. Rescue of conformational dynamics in enzyme catalysis by directed evolution. Nat. Commun. 9, 1–11.
Plevin, M.J., Bryce, D.L., Boisbouvier, J., 2010. Direct detection of CH/π in teractions in proteins. Nat. Chem. 2, 466–471.
Quinn, D.M., 1987. Acetylcholinesterase: enzyme structure, reaction dynamics, and virtual transition states. Chem. Rev. 87, 955–979.
Tormos, J.R., Wiley, K.L., Wang, Y., Fournier, D., Masson, P., Nachon, F., Quinn, D.M., 2010. Accumulation of tetrahedral intermediates in cholinesterase catalysis: a secondary isotope effect study. J. Am. Chem. Soc. 132, 17751–17759.
Weiss, M.S., 2001. Global indicators of X-ray data quality. J. Appl. Crystallogr. 34, 130–135.
Winn, M.D., Ballard, C.C., Cowtan, K.D., Dodson, E.J., Emsley, P., Evans, P.R., Keegan, R.M., Krissinel, E.B., Leslie, A.G.W., McCoy, A., McNicholas, S.J., Murshudov, G.N., Pannu, N.S., Potterton, E.A., Powell, H.R., Read, R.J., Vagin, A., Wilson, K.S., 2011. Overview of the CCP4 suite and current developments. Acta Crystallogr. D 67, 235–242.
wwPDB consortium. Protein Data Bank: the single global archive for 3D macromolecular structure data. Nucleic Acids Res. 47, 2019, D520–D528.